How to cite: *Angew. Chem. Int. Ed.* **2022,** *61,* e202208930
International Edition: doi.org/10.1002/anie.202208930
German Edition: doi.org/10.1002/ange.202208930

Coordination Chemistry

Isolation and Reactivity of Tetrylene-Tetrylone-Iron Complexes Supported by Bis(*N*-Heterocyclic Imine) Ligands

*Xuan-Xuan Zhao, Tibor Szilvási, Franziska Hanusch, John A. Kelly, Shiori Fujimori, and Shigeyoshi Inoue**

Dedicated to Professor Norihiro Tokitoh on the occasion of his 65th birthday

Abstract: The germanium iron carbonyl complex **3** was prepared by the reaction of dimeric chloro(imino)germylene $[IPrNGeCl]_2$ (IPrN = bis(2,6-diisopropylphenyl)imidazolin-2-iminato) with one equivalent of Collman's reagent ($Na_2Fe(CO)_4$) at room temperature. Similarly, the reaction of chloro(imino)stannylene $[IPrNSnCl]_2$ with $Na_2Fe(CO)_4$ (1 equiv) resulted in the $Fe(CO)_4$-bridged bis(stannylene) complex **4**. We observed reversible formation of bis(tetrylene) and tetrylene-tetrylone character in complexes **3** vs. **5** and **4** vs. **6**, which was supported by DFT calculations. Moreover, the Li/Sn/Fe trimetallic complex **12** has been isolated from the reaction of $[IPrNSnCl]_2$ with cyclopentadienyl iron dicarbonyl anion. The computational analysis further rationalizes the reduction pathway from these chlorotetrylenes to the corresponding complexes.

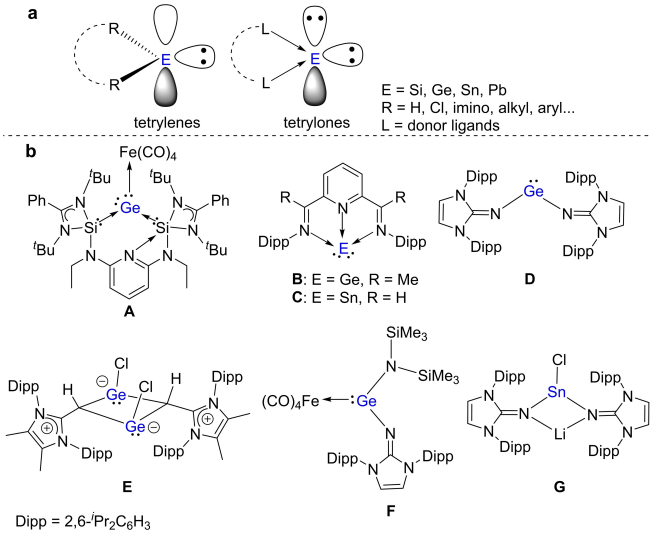

Figure 1. a) Electronic structures of tetrylenes (left) and tetrylones (right). b) Selected examples of low-valent germanium and tin compounds.

Introduction

Low-valent heavy Group 14 compounds are of great interest in contemporary research, due to their intriguing bonding, structures, and transition metal-like reactivity.[1] Monomeric divalent compounds of the heavier Group 14 elements (also known as tetrylenes), possess a lone pair of electrons and a vacant *p*-orbital (Figure 1a, left), and as a consequence have seen use in applications including small molecule activation, catalysis, and coordination chemistry.[2] Zerovalent compounds of Group 14 (tetrylones), in which the central tetrel atom is stabilized by two ligands via a donor-acceptor interaction, possess four valence electrons in the form of two lone pairs of electrons (Figure 1a, right).[3] Over the past two decades, the isolation and reactivity of tetrylones has garnered much attention.

Figure 1 outlines recently reported low-valent germanium and tin compounds supported by various donor ligands.[4,5] For instance, in 2016, Driess and co-workers reported the bis(silylenyl)pyridine-stabilized germylone iron carbonyl complex **A** and its tin derivative (Figure 1b).[6] In addition, two acceptor free E^0 compounds (E = Ge (**B**), Sn (**C**)) stabilized by a bis(imino)pyridine pincer ligand were isolated by Nikonov, Fischer and Flock et al., respectively.[4e,j] More recently, Rivard and co-workers reported on the synthesis of the dimeric Ge^{II} species **E** (Figure 1b), in which the two Ge centers are linked by anionic *N*-heterocyclic olefin (NHO) ligands.[4n]

Ligand design plays an integral role in modern main group chemistry, with the use of functional ligands providing access to various reactive low-coordinate compounds. *N*-

[*] X.-X. Zhao, Dr. F. Hanusch, Dr. J. A. Kelly, Dr. S. Fujimori, Prof. Dr. S. Inoue
School of Natural Sciences, Department of Chemistry, WACKER-Institute of Silicon Chemistry and Catalysis Research Center, Technische Universität München
Lichtenbergstraße 4, 85748 Garching bei München (Germany)
E-mail: s.inoue@tum.de
Prof. Dr. T. Szilvási
Department of Chemical and Biological Engineering, University of Alabama
Tuscaloosa, AL 35487 (USA)

heterocyclic imine (NHI) ligands may act as a 2σ- and either 2π- or 4π electron donors.[7] Therefore, the imino group is an excellent choice for thermodynamic stabilization of electron-deficient species. For example, in 2015, the Rivard group described the synthesis of a two-coordinate acyclic germylene **D** supported by two NHI ligands.[8] Recently, we have developed a number of synthetic methods to stabilize low-coordinate Group 14 element compounds using NHIs as supporting ligands.[9b,10] For example, we reported the germylene iron carbonyl complex **F** with a trigonal planar-coordinate germanium atom,[10b] and also a rare example of the lithium bis(imino)stannylenoid **G** as a heavier carbenoid congener.[9] To expand this chemistry, we were interested in exploring the synthetic potential of dimeric chloro-(imino)tetrylenes as a precursor for novel low-valent species for applications in bond activation and catalysis.

We have previously reported the isolation of dimeric chloro(imino)stannylene **2** (Scheme 1), but its reactivity has not yet been explored.[9b,10g] Continuing this study, herein we show a simplified route to the chlorotetrylenes **1** and **2**, and report on tetrylene-tetrylone complexes prepared by the reaction of chlorotetrylenes with anionic iron carbonyls ($Na_2Fe(CO)_4$ and $M[Fe(CO)_2(\eta^5\text{-}C_5H_5)]$, M = Li, K).

Results and Discussion

The reaction of ECl_2·dioxane (E = Ge, Sn) with one equivalent of IPrNLi (IPrN = bis(2,6-diisopropylphenyl)imidazolin-2-iminato) in THF at room temperature led to the corresponding chlorotetrylenes $[IPrNECl]_2$ **1** (E = Ge) and **2** (E = Sn) in high yields (**1**: 97 % and **2**: 67 %; Scheme 1). Compounds **1** and **2** are soluble in polar solvents such as chloroform and acetonitrile, but dissolve poorly in nonpolar hydrocarbons. The structure of **1** and **2** were both characterized by multinuclear NMR spectroscopy and elemental analysis (EA).

Single crystal X-ray diffraction (SC-XRD) analysis of **1** revealed that the molecular structure in the solid state comprises of a centrosymmetric dimer, with a planar and rhombic N_2Ge_2 ring (sum of internal tetragonal angles: 360°, Figure 2). The Ge–Cl bonds adopt a *trans* configuration with respect to the Ge_2N_2 ring. In comparison, Rivard's NHO–Ge^{II} dimer **E** contains a puckered Ge_2N_2 ring, which is capped by *syn*-arranged Ge–Cl bonds. The Ge–N bond lengths of 1.956(7) Å and 2.003(7) Å are significantly longer than that in $[IPrN]_2Ge$ (**D**) [1.8194(15) Å] and **F** [1.755 (2) Å]. They are comparable to that in imino-stabilized Ge^{II} monocation[10b] [1.9694(14) Å] and **B** [Ge–N_{imino} 2.047(7) Å], indicating a partial dative bond character for the germanium-nitrogen interactions in **1**. The structural features are very similar to that seen in **2**.[9b] However, further structure discussion is restricted, due to enlarged thermal ellipsoids and disorder resulting from data collection at 200 K.

Treating chlorogermylene **1** with $Na_2Fe(CO)_4$ (1 equiv) results in the formation of germanium iron carbonyl complex **3**, isolated in good yield (82 %) as a red crystalline solid (Scheme 1). The CO-signal of the $Fe(CO)_4$ moiety in the $^{13}C\{^1H\}$ NMR spectrum (C_6D_6) appears at 217.7 ppm and the solid state IR spectrum shows the characteristic CO stretching vibration of **3** at 1975, 1909, 1877, and 1862 cm^{-1}, which are comparable to those in complex **A** [1969, 1886, 1865, and 1830 cm^{-1}], but are red-shifted compared to those in **F** [2039, 1965, and 1930 cm^{-1}],[10b] suggesting that the carbonyl groups experience a strong electron back-donation.

The molecular structure and Density Functional Theory (DFT) calculations revealed that complex **3** contains two Ge^{II} atoms, bridged by a $Fe(CO)_4$ moiety (Figure 3). The Ge1 center adopts a trigonal-pyramidal geometry (sum of the angles around the Ge1 atom: 260.33°), which is similar to that in bis(*N*-heterocyclic carbene) supported germylone-$GaCl_3$ adduct (266.33°)[4g] and complex **A** (322.59°), but different from the trigonal planar Ge moiety in **F**. The Ge1–Fe1 bond length of 2.6968(6) Å is longer than that in **A** [2.4987(5) Å] and **F** [2.3026(5) Å]. Moreover, the X-ray structure of **3** revealed a Ge2···Fe1 distance of 2.9670(5) Å, and a wider angle of C55–Fe1–C57 (144.23°) than the expected 120°, thus indicating a weak interaction between

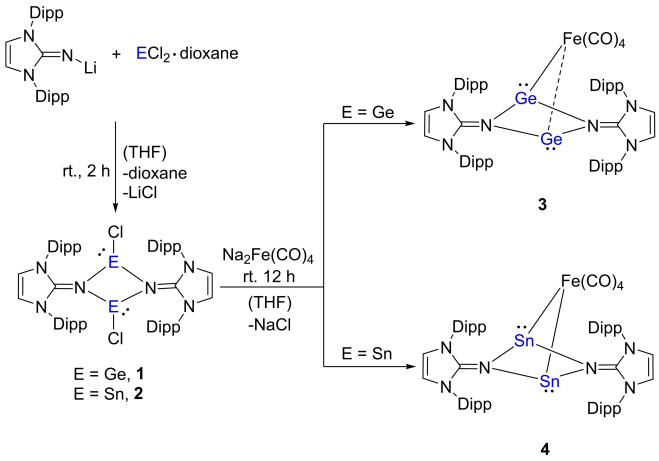

Scheme 1. Synthesis of $Fe(CO)_4$-bridged germanium and tin complexes **3** and **4** from chloro(imino)tetrylenes **1** and **2**, respectively.

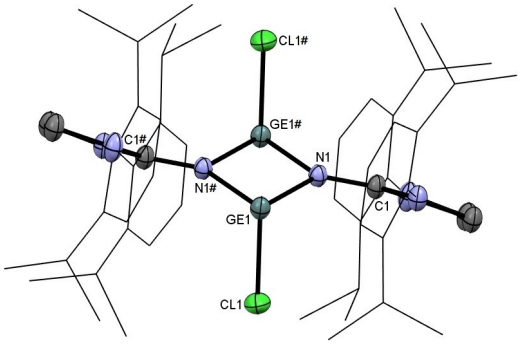

Figure 2. Molecular structure of **1**.[13] Thermal ellipsoids are shown at 30 % probability level. Hydrogen atoms are omitted for clarity. Selected bond lengths [Å] and angles [°]: Ge1–Cl1 2.385(7), Ge1–N1 1.956(7), N1–C1 1.305(13), Ge1–N1# 2.003(7), Cl1–Ge1–N1 94.0(3), Cl1–Ge1–N1# 89.5(3), N1–Ge1–N1# 79.5(3), Ge1–N1–C1 131.2(6), Ge1–N1#–C1# 127.6(6), Ge1–N1–Ge1# 100.5(4).

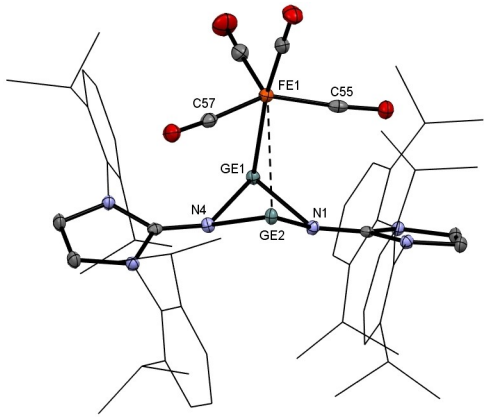

Figure 3. Molecular structure of **3**.[13] Thermal ellipsoids are shown at 50% probability level. Hydrogen atoms and solvent molecules are omitted for clarity. Selected bond lengths [Å] and angles [°]: Ge1–Fe1 2.6968(6), Ge2···Fe1 2.9670(5), Ge1–N1 2.0601(12), Ge1–N4 2.0219 (12), Ge2–N1 1.9585(12), Ge2–N4 1.9888(13), C1–N1 1.3066(18), C4–N4 1.3042(18), Fe1–Ge1–N1 92.37(4), Fe1–Ge1–N4 91.80(4), N1–Ge1–N4 76.16(5), N1–Ge2–N4 79.26(5), Ge1–N1–Ge2 87.03(5), Ge1–N4–Ge2 87.27(5), Ge1–N1–C1 132.59(9), Ge1–N4–C4 134.85 (10), Ge2–N1–C1 126.98(9), Ge2–N4–C4 125.76(9), C55–Fe1–C57 144.23.

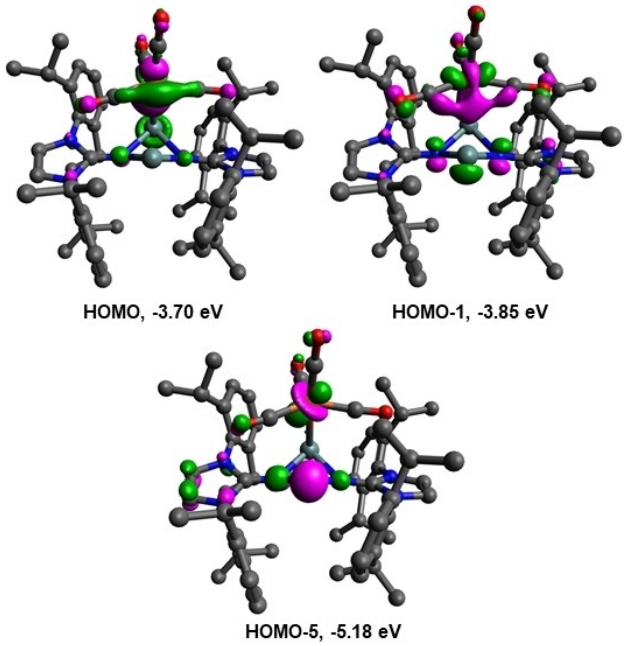

Figure 4. Molecular orbitals of **3**. Hydrogens are omitted for clarity.

Fe1 and Ge2. The Ge1–N1 and Ge1–N4 bond lengths [2.0601(12) Å and 2.0219(12) Å] are almost identical to that in Nikonov's germylone **B** [Ge–N_{imino} 2.047(7) Å]. Accordingly, the Ge2–N_{imino} distances are increased with respect to Rivard's bis(imino)germylene **D** [1.9585(12) Å and 1.9888 (13) Å vs. 1.8194(15) Å]. The Ge1···Ge2 separation in **3** [2.7678 Å] is consistent with an absence of Ge1–Ge2 bonding (sum of two Ge covalent radii = 2.44 Å).[11] In addition, the N1–Ge2–N4 angle of 79.26(5)° is considerably more acute than that in **D** [99.48(10)°].

To gain further insight into the electronic structure and bonding of **3**, DFT calculations were carried out at the ωB97X–D/def2-TZVPP//B97-D/def2-SVP level of theory. Natural Bond Orbital (NBO) analysis of **3** shows N centered lone pairs and empty Ge orbitals (Table S8) indicating donation from the nitrogen to the germanium center. Analysis of the frontier orbitals (Figure 4) shows that HOMO and HOMO-5 depict lone pairs of electrons on the Ge centers while HOMO-1 and HOMO-5 feature out-of-plane (π) and in-plane (σ) type contribution from the N atoms.

Similarly, the chlorostannylene **2** was treated with $Na_2Fe(CO)_4$ (1 equiv) to give the $Fe(CO)_4$-bridged bis(stannylene) complex **4** in 74% yield (Scheme 1). The $^{13}C\{^1H\}$ NMR spectrum (C_6D_6) of **4** displays one carbonyl signal at 216.9 ppm. The characteristic iron-carbonyl vibrations were found at 1976, 1899, and 1870 cm^{-1} in the solid-state IR spectrum. Analysis of the frontier orbitals (Figure 5) shows that the HOMO and HOMO-5 depict lone pairs of electrons on the Sn centers.

SC-XRD analysis of **4** revealed that the $Fe(CO)_4$ fragment bridges the two tin(II) centers with bond lengths 2.8511(10) Å (Sn1–Fe1) and 2.9432(10) Å (Sn2–Fe1) (Figure 6). Notably, the imino groups link the two Sn atoms almost symmetrically in the N_2Sn_2 ring [bond lengths for Sn–N: 2.204(3) Å, 2.240(3) Å, 2.237(3) Å and 2.180(3) Å]. One signal (357.3 ppm, C_6D_6) was observed in the $^{119}Sn\{^1H\}$ NMR spectrum, which is confirmed by Gauge-Independent Atomic Orbital (GIAO) calculations ($\delta_{calcd.}$ = 360 ppm). This indicates the Sn–Fe bond lengths equilibrate in solution.

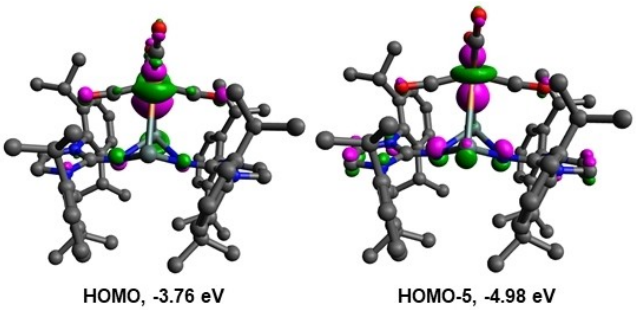

Figure 5. Molecular orbitals of **4**. Hydrogens are omitted for clarity.

In addition, NBO analysis shows only one Ge–Fe bond in **3**, whereas each Sn center has one bond with Fe in **4** (Table S8 and Table S9). Wiberg Bond Index (WBI) indicates weak E–Fe (E = Ge or Sn) single bonds (≈0.40–0.58, Table S10) which are consistent with the large polarization of the E–Fe bonds (Fe1 in **3**: 65.50%; Fe1 in **4**: 88.02% and 66.29%). Second order perturbation analysis of the Ge2 vacant orbital and Fe1 lone pair of electrons shows large donor-acceptor stabilization energy of 57.10 kcal mol^{-1}. DFT analysis indicates an equilibrium between **3** and **4** with their respective monocoordinated structures **5** and **6** (Scheme 2), whereby the $Fe(CO)_4$ fragment sits almost perpendicular to the N_2E_2 ring bound to only one tetrel

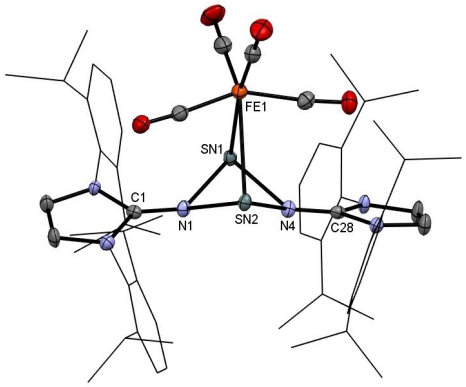

Figure 6. Molecular structure of **4**.[13] Thermal ellipsoids are shown at 50% probability level. Hydrogen atoms are omitted for clarity. Selected bond lengths [Å] and angles [°]: Sn1–Fe1 2.8511(10), Sn2–Fe1 2.9432 (10), Sn1–N1 2.204(3), Sn1–N4 2.240(3), Sn2–N1 2.237(3), Sn2–N4 2.180(3), N1–C1 1.291(5), N4–C28 1.300(5), Sn1–Fe1–Sn2 64.65(2), Fe1–Sn1–N1 86.97(8), Fe1–Sn1–N4 87.21(8), Fe1–Sn2–N1 84.13(8), Fe1–Sn2–N4 86.03(9), Sn1–N1–Sn2 88.51(11), Sn1–N4–Sn2 89.05 (10), N1–Sn1–N4 75.80(10), N1–Sn2–N4 76.35(11), Sn1–N1–C1 130.2(2), Sn1–N4–C28 129.6(3), Sn2–N1–C1 129.5(2), Sn2–N4–C28 129.7(3).

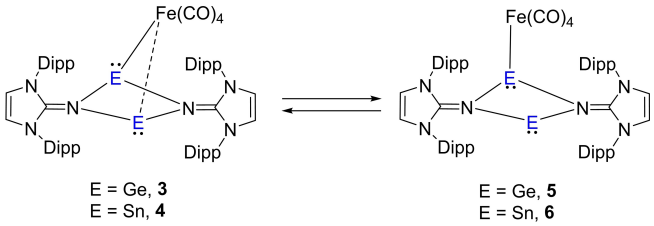

Scheme 2. Temperature-dependent exchange of the E–Fe bonding (E = Ge, Sn).

atom (see Supporting Information for calculated structures of **5** and **6**, Figure S55 and Figure S56, respectively). The variable temperature (VT) ^{119}Sn NMR analysis of **4** shows the signal is high field shifted and broadens at lower temperatures, possibly showing the monocoordinated **6** being "frozen out" at lower temperatures in solution (Figure S22). GIAO NMR calculations indicate that the values for the different Sn centers in both the mono-coordinate and bridged species are almost equivalent.

To investigate the reactivity of these complexes, **3** was treated with two equivalents of $GaCl_3$ in C_6D_6 which led to the formation of complex $[(IPrNGe)_2(\mu\text{-}Cl)][GaCl_4]$ **7** (Scheme 3). The yellow-orange solid was identified by multinuclear NMR spectroscopy and single-crystal X-ray diffraction (see Supporting Information for details). Compound **7** is comparable to that of Rivard's complex, $[\{(^{Me}IPrCH)Ge\}_2(\mu\text{-}Cl)][BAr^F{}_4]$ [Ar^F = 3,5-$(CF_3)_2$-C_6H_3].[4n] Similarly, treatment of **4** with $GaCl_3$ (2 equiv) resulted in complex **8** as an orange-red solid (Scheme 3). The ^{119}Sn{^{1}H} NMR spectrum of **8** in THF-d_8 shows a signal at σ = 139.6 ppm that is shifted to higher field compared to that of **4** (357.3 ppm, C_6D_6).

Motivated by the above results, we investigated the reactivity of **1** and **2** towards $K[Fe(CO)_2(\eta^5\text{-}C_5H_5)]$ (FpK).

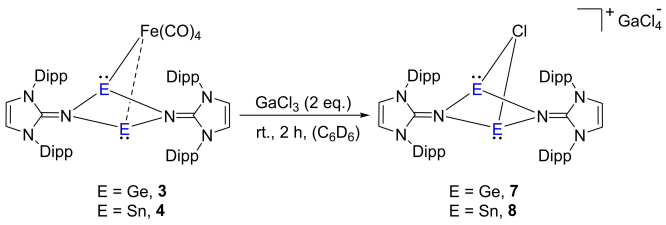

Scheme 3. Reaction of **3** and **4** with $GaCl_3$ to **7** and **8**.

Reaction of **1** with three equivalents of FpK resulted in a complex product mixture which contains **D**, large amount of free ligand IPrNH, and other undefined species. Similarly, treatment of **2** with FpK (3 equiv) in THF led to the formation of a complicated mixture of products. However, the one-pot reaction of IPrNLi and $GeCl_2$·dioxane with three equivalents of FpK in THF, forms already reported bis(imino)germylene **D** in reasonable yields (62%) confirmed by ^{1}H NMR spectroscopy.[8] In comparison, the reaction of **2** with FpK (3 equiv) in THF resulted in the Li/Sn/Fe trimetallic complex **12** in 60% yield (Scheme 4). In addition, the isolated yields of **D** and **12** did not significantly deviate if isolated **1** and **2** reacted directly with $Li[Fe(CO)_2(\eta^5\text{-}C_5H_5)]$ (FpLi, 3 equiv) instead of the in situ protocol.

The formation of bis(imino)germylene **D** can be rationalized by the release of Ge metal via the intermediate **9**. Notably, the reduction of **E** led to similar disproportionation products (Ge metal and R_2Ge:, R = NHO).[4n] It appears that the plausible intermediate **10** readily decomposes to yield Sn metal and the bis(imino)stannylene **11**, which can react with FpLi to yield complex **12** (Scheme 4). To clarify the mechanism, we performed the reaction of isolated **11** with FpLi (1 equiv) at room temperature, which formed the desired product **12** in nearly quantitative yield. No reaction was observed between **D** and FpLi even at elevated temperatures. All attempts to isolate **9** and **10** by reducing the corresponding chlorotetrylenes **1** and **2** with common

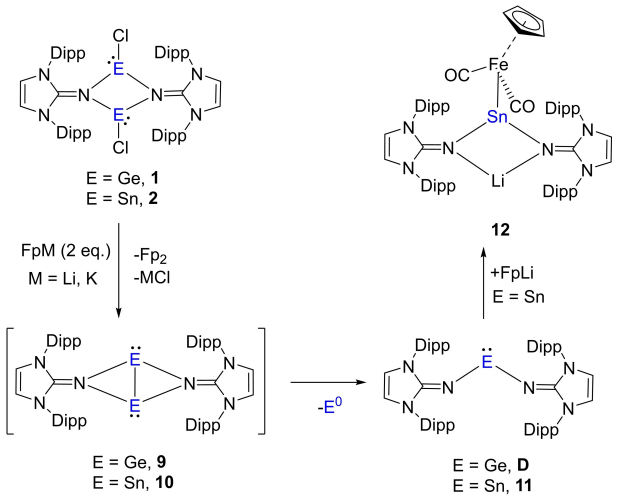

Scheme 4. Reaction of chloro(imino)tetrylenes **1** and **2** with $M[Fe(CO)_2(\eta^5\text{-}C_5H_5)]$ (M = Li, K), as well as proposed mechanism.

reducing agents (such as K, KC_8) have so far been unsuccessful.

Computational analysis using DFT was carried out to understand the reduction pathway from chloro-(imino)tetrylenes $[IPrNECl]_2$ (E = Ge, **1**; Sn, **2**) to bis-(imino)tetrylenes $[IPrN]_2E$ (E = Ge, **D**; Sn, **11**) and bulk E metal (Figure S48). We found that the reduction of **1** and **2** to **9** and **10** is strongly favored in internal energy similar to the Ge/Sn metal deposition (−58.4/−42.2 kcal mol^{-1}) that drives the reaction toward **D** and **11** (Figure S48). In addition, we have also studied possible intermediates with different geometry and canonical forms during the reduction reaction (Scheme 5). Interestingly, our calculations indicate that both type **II** and **III** structures converge to **I**, which is equivalent to **9** and **10** and has a more butterfly structure compared to **II** and **III**, without having a local minimum for type **II** and **III** structures. We have also considered Fp as a substituent for **9** and **10** (Figure S48). Computations showed the dissociation of the Fe-substituted dimer (**IV**) presumably due to steric reasons, however the formation of its monomer is thermodynamically favored, although it is less favorable than the experimentally observed metal deposition. The acyclic E(I) dimers (**V**) are less stable by more than 15 kcal mol^{-1} than **I**.

Interestingly, the lithium stannylenoid (**G**) is energetically favored relative to the corresponding lithium germylenoid (−1.6 kcal mol^{-1} vs. +8.5 kcal mol^{-1}, Figure S48). In addition, we found that the potassium derivative of **12** is less stable than the lithium analogue (−50.4 kcal mol^{-1} vs. −63.4 kcal mol^{-1}). The product derived from insertion of the Sn center in compound **11** into the Fe–Li bond of FpLi is higher by +41.8 kcal mol^{-1} in energy than its isomer **12** (Figure S48).

Complex **12** has a relatively high thermal stability in C_6D_6, with no elimination of FpLi observed even after heating to 80 °C for 16 hours. However, treatment of **12** with N_2O immediately resulted in the formation of **11**, which then further reacts with N_2O leading to decomposition products. The $^{119}Sn\{^1H\}$ NMR spectrum of **12** in C_6D_6 displays a singlet at 314.0 ppm, which is significantly shifted to lower field as compared to **G** [−52.1 ppm, C_6D_6], but higher field shifted compared to Power's ferrio-stannylene $ArSnFe(CO)_2(\eta^5\text{-}C_5H_5)$ (Ar = 2,6-(2,6-^{i}Pr$_2$C$_6$H$_3$)$_2$C$_6$H$_3$) [2951 ppm, C_6D_6].[12c] The iron-carbonyl (CO) signal in the $^{13}C\{^1H\}$ NMR spectrum (C_6D_6) appears at 222.6 ppm. The CO stretching vibration was found at 2006 and 1925 cm^{-1} in the solid state IR spectrum, which is comparable to that in ferrio-stannylene [1970 and 1921 cm^{-1}] and Driess's iron-stannylene complex $LSnFe(CO)_2(\eta^5\text{-}C_5H_5)$ (L = β-diketiminate) [1961 and 1907 cm^{-1}].[12b]

SC-XRD study revealed that **12** contains a four-membered LiN_2Sn ring, in which the sum of the internal bond angles amounts to 354.83° (Figure 7). The Sn–N bond lengths [2.1763(11) Å and 2.1717(11) Å] in **12** are comparable to that in **G** [2.143(5) Å and 2.179(4) Å]. The Sn1–Fe1 bond length [2.7671(6) Å] is significantly elongated in comparison to that in the ferrio-stannylene [2.5634(5) Å], but shorter than those in **4** [2.8511(10) Å and 2.9432(10) Å].

Treatment of **12** with the nucleophilic reagent LiI (1 equiv) afforded the iodo-substituted tin complex **13** (Scheme 6). The formation of **13** demonstrates the electrophilicity of the tin(II) center in **12**. In the $^{119}Sn\{^1H\}$ NMR spectrum, one signal appears at σ = 61.6 ppm (C_6D_6), which is shifted upfield in comparison to **12** [314.0 ppm, C_6D_6], presumably because the electron-donating capacity of the iodide is higher than that of the Fp group.

The molecular structure of **13** was also determined by single crystal X-ray diffraction analysis (Figure 8). The

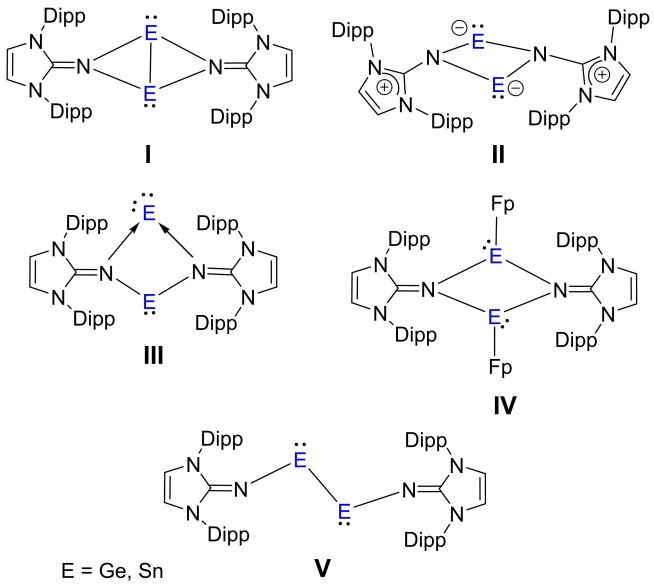

Scheme 5. Potential intermediates in the reaction of **1** and **2** with FpM (M = Li, K).

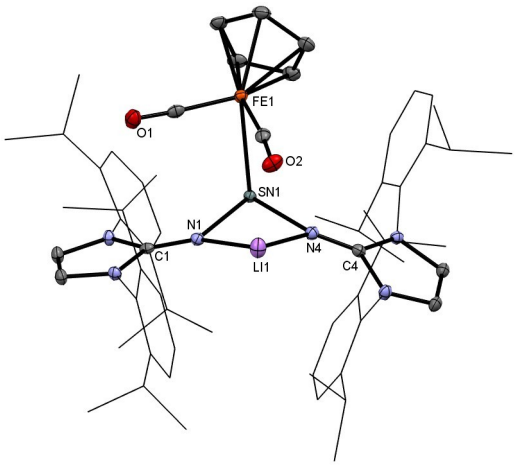

Figure 7. Molecular structure of **12**.[13] Thermal ellipsoids are shown at 50% probability level. Hydrogen atoms and solvent molecules are omitted for clarity. Selected bond lengths [Å] and angles [°]: Sn1–Fe1 2.7671(6), Sn1–N1 2.1763(11), Sn1–N4 2.1717(11), Li1–N1 1.950(3), Li1–N4 1.945(3), C1–N1 1.2713(18), C4–N4 1.2650(18), Fe1–Sn1–N1 96.24(3), Fe1–Sn1–N4 100.66(3), Sn1–N1–C1 129.16(9), Sn1–N4–C4 132.68(9), Li1–N1–C1 141.33(12), Li1–N4–C4 134.92(12), Sn1–N1–Li1 89.40(9), Sn1–N4–Li1 89.66(9), N1–Sn1–N4 81.83(4), N1–Li1–N4 93.94(11).

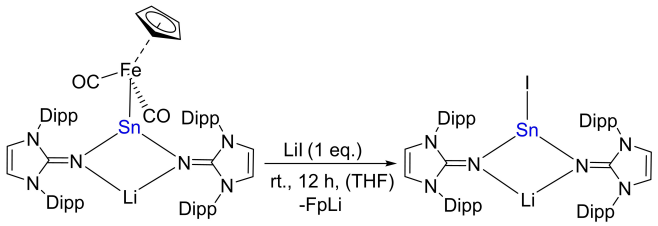

Scheme 6. Reaction of **12** with LiI to **13**.

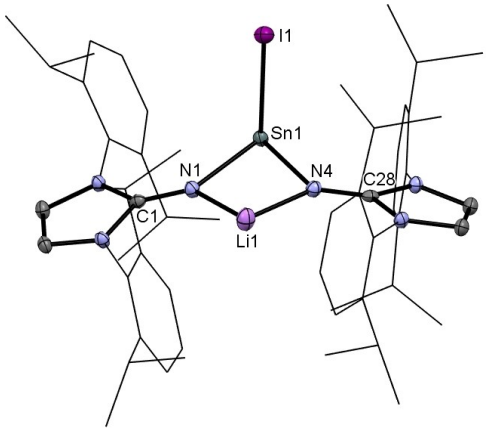

Figure 8. Molecular structure of **13**.[13] Thermal ellipsoids are shown at 50% probability level. Hydrogen atoms and solvent molecules are omitted for clarity. Selected bond lengths [Å] and angles [°]: Sn1–I1 3.0218(6), Sn1–N1 2.136(2), Sn1–N4 2.136(2), Li1–N1 1.944(4), Li1–N4 1.923(4), C1–N1 1.273(3), C28–N4 1.278(2), I1–Sn1–N1 98.13(5), I1–Sn1–N4 88.86(5), Sn1–N1–C1 135.8(1), Sn1–N4–C28 130.7(1), Li1–N1–C1 131.0(2), Li1–N4–C28 135.7(2), Sn1–N1–Li1 93.0(1), Sn1–N4–Li1 93.6(1), N1–Sn1–N4 80.48(6), N1–Li1–N4 91.1(2).

structural features are very similar to that seen in **G** and **12**. The Sn–I bond in **13** is oriented nearly perpendicular to both Sn–N bonds, with I1–Sn1–N1 and I1–Sn1–N4 bond angles of 98.13(5) and 88.86(5), respectively.

Conclusion

In summary, we have reported on the synthesis of the centrosymmetric chloro(imino)tetrylenes $[IPrNECl]_2$ (E = Ge (**1**), Sn (**2**)), with a planar and rhombic N_2E_2 ring. The reaction of $[IPrNECl]_2$ with one equivalent of $Na_2Fe(CO)_4$ led to the corresponding germanium and tin iron carbonyl complexes. Notably, the $Fe(CO)_4$ fragment shows different bonding situations in solution and solid state of these complexes (E–Fe bonding: mono-coordinate vs. bridged, E = Ge, Sn). Moreover, we isolated the Li/Sn/Fe trimetallic complex **12** by the reaction of chloro(imino)stannylene **2** with $K[Fe(CO)_2(\eta^5\text{-}C_5H_5)]$. Further coordination chemistry, bond activation and catalytic applications of these low-valent compounds are currently under investigation.

Acknowledgements

We gratefully acknowledge financial support from the Deutsche Forschungsgemeinschaft (In 234/7-1). X.Z. gratefully acknowledges financial support from the China Scholarship Council. We thank Dr. Christian Jandl for the SC-XRD measurements of compound **3** and **12**. We thank Florian Tschernuth for the VT NMR measurements, as well as Maximilian Muhr for the LIFDI-MS measurements. Open Access funding enabled and organized by Projekt DEAL.

Conflict of Interest

The authors declare no conflict of interest.

Data Availability Statement

The data that support the findings of this study are available in the Supporting Information of this article.

Keywords: Germanium · Iron Carbonyl Complexes · Low-Valent Compounds · Tin · Trimetallic Complexes

[1] a) P. P. Power, *Nature* **2010**, *463*, 171–177; b) D. Martin, M. Soleilhavoup, G. Bertrand, *Chem. Sci.* **2011**, *2*, 389–399; c) C. Weetman, S. Inoue, *ChemCatChem* **2018**, *10*, 4213–4228; d) T. J. Hadlington, M. Driess, C. Jones, *Chem. Soc. Rev.* **2018**, *47*, 4176–4197; e) R. L. Melen, *Science* **2019**, *363*, 479–484; f) F. Hanusch, L. Groll, S. Inoue, *Chem. Sci.* **2021**, *12*, 2001–2015; g) M. M. D. Roy, A. A. Omana, A. S. S. Wilson, M. S. Hill, S. Aldridge, E. Rivard, *Chem. Rev.* **2021**, *121*, 12784–12965.

[2] a) M. Veith, *Angew. Chem. Int. Ed. Engl.* **1987**, *26*, 1–14; *Angew. Chem.* **1987**, *99*, 1–14; b) W. P. Neumann, *Chem. Rev.* **1991**, *91*, 311–334; c) H. V. R. Dias, Z. Y. Wang, W. C. Jin, *Coord. Chem. Rev.* **1998**, *176*, 67–86; d) M. Weidenbruch, *Eur. J. Inorg. Chem.* **1999**, 373–381; e) N. Tokitoh, R. Okazaki, *Coord. Chem. Rev.* **2000**, *210*, 251–277; f) O. Kühl, *Coord. Chem. Rev.* **2004**, *248*, 411–427; g) I. Saur, S. G. Alonso, J. Barrau, *Appl. Organomet. Chem.* **2005**, *19*, 414–428; h) W. P. Leung, K. W. Kan, K. H. Chong, *Coord. Chem. Rev.* **2007**, *251*, 2253–2265; i) S. Nagendran, H. W. Roesky, *Organometallics* **2008**, *27*, 457–492; j) A. V. Zabula, F. E. Hahn, *Eur. J. Inorg. Chem.* **2008**, 5165–5179; k) Y. Mizuhata, T. Sasamori, N. Tokitoh, *Chem. Rev.* **2009**, *109*, 3479–3511; l) M. Asay, C. Jones, M. Driess, *Chem. Rev.* **2011**, *111*, 354–396; m) S. Khan, *Adv. Organomet. Chem.* **2020**, *74*, 105–152.

[3] a) N. Takagi, T. Shimizu, G. Frenking, *Chem. Eur. J.* **2009**, *15*, 8593–8604; b) D. J. Wilson, J. L. Dutton, *Chem. Eur. J.* **2013**, *19*, 13626–13637; c) G. Frenking, M. Hermann, D. M. Andrada, N. Holzmann, *Chem. Soc. Rev.* **2016**, *45*, 1129–1144; d) S. Yao, Y. Xiong, M. Driess, *Acc. Chem. Res.* **2017**, *50*, 2026–2037; e) L. Zhao, M. Hermann, N. Holzmann, G. Frenking, *Coord. Chem. Rev.* **2017**, *344*, 163–204; f) P. K. Majhi, T. Sasamori, *Chem. Eur. J.* **2018**, *24*, 9441–9455; g) S. Yao, Y. Xiong, A. Saddington, M. Driess, *Chem. Commun.* **2021**, *57*, 10139–10153.

[4] a) T. Iwamoto, H. Masuda, C. Kabuto, M. Kira, *Organometallics* **2005**, *24*, 197–199; b) T. Iwamoto, T. Abe, C. Kabuto, M. Kira, *Chem. Commun.* **2005**, 5190–5192; c) Y. Xiong, S.

Yao, G. Tan, S. Inoue, M. Driess, *J. Am. Chem. Soc.* **2013**, *135*, 5004–5007; d) Y. Li, K. C. Mondal, H. W. Roesky, H. Zhu, P. Stollberg, R. Herbst-Irmer, D. Stalke, D. M. Andrada, *J. Am. Chem. Soc.* **2013**, *135*, 12422–12428; e) T. Chu, L. Belding, A. van der Est, T. Dudding, I. Korobkov, G. I. Nikonov, *Angew. Chem. Int. Ed.* **2014**, *53*, 2711–2715; *Angew. Chem.* **2014**, *126*, 2749–2753; f) B. Su, R. Ganguly, Y. Li, R. Kinjo, *Angew. Chem. Int. Ed.* **2014**, *53*, 13106–13109; *Angew. Chem.* **2014**, *126*, 13322–13325; g) Y. Xiong, S. Yao, M. Karni, A. Kostenko, A. Burchert, Y. Apeloig, M. Driess, *Chem. Sci.* **2016**, *7*, 5462–5469; h) Y. Wang, M. Karni, S. Yao, Y. Apeloig, M. Driess, *J. Am. Chem. Soc.* **2019**, *141*, 1655–1664; i) M. T. Nguyen, D. Gusev, A. Dmitrienko, B. M. Gabidullin, D. Spasyuk, M. Pilkington, G. I. Nikonov, *J. Am. Chem. Soc.* **2020**, *142*, 5852–5861; j) J. Flock, A. Suljanovic, A. Torvisco, W. Schoefberger, B. Gerke, R. Pottgen, R. C. Fischer, M. Flock, *Chem. Eur. J.* **2013**, *19*, 15504–15517; k) T. Kuwabara, M. Nakada, J. Hamada, J. D. Guo, S. Nagase, M. Saito, *J. Am. Chem. Soc.* **2016**, *138*, 11378–11382; l) Z. Dong, K. Bedbur, M. Schmidtmann, T. Muller, *J. Am. Chem. Soc.* **2018**, *140*, 3052–3060; m) V. Nesterov, R. Baierl, F. Hanusch, A. E. Ferao, S. Inoue, *J. Am. Chem. Soc.* **2019**, *141*, 14576–14580; n) E. Hupf, F. Kaiser, P. A. Lummis, M. M. D. Roy, R. McDonald, M. J. Ferguson, F. E. Kuhn, E. Rivard, *Inorg. Chem.* **2020**, *59*, 1592–1601; o) D. Sarkar, C. Weetman, D. Munz, S. Inoue, *Angew. Chem. Int. Ed.* **2021**, *60*, 3519–3523; *Angew. Chem.* **2021**, *133*, 3561–3565; p) S. Yao, A. Kostenko, Y. Xiong, C. Lorent, A. Ruzicka, M. Driess, *Angew. Chem. Int. Ed.* **2021**, *60*, 14864–14868; *Angew. Chem.* **2021**, *133*, 14990–14994; q) A. Caise, L. Griffin, A. Heilmann, C. McManus, J. Campos, S. Aldridge, *Angew. Chem. Int. Ed.* **2021**, *60*, 15606–15612; *Angew. Chem.* **2021**, *133*, 15734–15740.

[5] For selected examples of E_2N_2 and $E_4(NR)_4$ species in Group 14 elements, and coordination of low-valent germanium to iron, see: a) M. Veith, S. Becker, V. Huch, *Angew. Chem. Int. Ed. Engl.* **1990**, *29*, 216–218; *Angew. Chem.* **1990**, *102*, 186–188; b) M. Veith, A. Rammo, *Z. Anorg. Allg. Chem.* **2001**, *627*, 662–668; c) E. H. Brooks, M. Elder, W. A. G. Graham, D. Hall, *J. Am. Chem. Soc.* **1968**, *90*, 3587–3588; d) C. Cui, M. Brynda, M. M. Olmstead, P. P. Power, *J. Am. Chem. Soc.* **2004**, *126*, 6510–6511; e) C. Cui, M. M. Olmstead, J. C. Fettinger, G. H. Spikes, P. P. Power, *J. Am. Chem. Soc.* **2005**, *127*, 17530–17541; f) J. F. Eichler, O. Just, W. S. Rees, Jr., *Inorg. Chem.* **2006**, *45*, 6706–6712; g) N. Wiberg, P. Karampatses, C. K. Kim, *Chem. Ber.* **1987**, *120*, 1203–1212; h) N. Wiberg, G. Preiner, P. Karampatses, C. K. Kim, K. Schurz, *Chem. Ber.* **1987**, *120*, 1357–1368; i) X. Wang, C. Ni, Z. Zhu, J. C. Fettinger, P. P. Power, *Inorg. Chem.* **2009**, *48*, 2464–2470; j) A. Jana, V. Huch, H. S. Rzepa, D. Scheschkewitz, *Organometallics* **2015**, *34*, 2130–2133; k) A. Jana, M. Majumdar, V. Huch, M. Zimmer, D. Scheschkewitz, *Dalton Trans.* **2014**, *43*, 5175–5181.

[6] a) Y. P. Zhou, M. Karni, S. Yao, Y. Apeloig, M. Driess, *Angew. Chem. Int. Ed.* **2016**, *55*, 15096–15099; *Angew. Chem.* **2016**, *128*, 15320–15323; b) J. Xu, C. Dai, S. Yao, J. Zhu, M. Driess, *Angew. Chem. Int. Ed.* **2022**, *61*, e202114073; *Angew. Chem.* **2022**, *134*, e202114073.

[7] a) T. Ochiai, D. Franz, S. Inoue, *Chem. Soc. Rev.* **2016**, *45*, 6327–6344; b) X. Wu, M. Tamm, *Coord. Chem. Rev.* **2014**, *260*, 116–138.

[8] a) M. W. Lui, C. Merten, M. J. Ferguson, R. McDonald, Y. Xu, E. Rivard, *Inorg. Chem.* **2015**, *54*, 2040–2049; b) X. Zhao, T. Szilvási, F. Hanusch, S. Inoue, *Chem. Eur. J.* **2021**, *27*, 15914–15917.

[9] For selected examples of stannylenoid, see: a) H. Arp, J. Baumgartner, C. Marschner, T. Muller, *J. Am. Chem. Soc.* **2011**, *133*, 5632–5635; b) T. Ochiai, D. Franz, X. N. Wu, E. Irran, S. Inoue, *Angew. Chem. Int. Ed.* **2016**, *55*, 6983–6987; *Angew. Chem.* **2016**, *128*, 7097–7101.

[10] a) S. Inoue, K. Leszczynska, *Angew. Chem. Int. Ed.* **2012**, *51*, 8589–8593; *Angew. Chem.* **2012**, *124*, 8717–8721; b) T. Ochiai, D. Franz, X. N. Wu, S. Inoue, *Dalton Trans.* **2015**, *44*, 10952–10956; c) T. Ochiai, D. Franz, E. Irran, S. Inoue, *Chem. Eur. J.* **2015**, *21*, 6704–6707; d) T. Ochiai, S. Inoue, *Phosphorus Sulfur Silicon Relat. Elem.* **2016**, *191*, 624–627; e) T. Ochiai, T. Szilvasi, D. Franz, E. Irran, S. Inoue, *Angew. Chem. Int. Ed.* **2016**, *55*, 11619–11624; *Angew. Chem.* **2016**, *128*, 11791–11796; f) T. Ochiai, T. Szilvasi, S. Inoue, *Molecules* **2016**, *21*, 1155–1167; g) T. Ochiai, S. Inoue, *RSC Adv.* **2017**, *7*, 801–804; h) D. Wendel, A. Porzelt, F. A. D. Herz, D. Sarkar, C. Jandl, S. Inoue, B. Rieger, *J. Am. Chem. Soc.* **2017**, *139*, 8134–8137; i) D. Wendel, T. Szilvasi, C. Jandl, S. Inoue, B. Rieger, *J. Am. Chem. Soc.* **2017**, *139*, 9156–9159; j) D. Wendel, T. Szilvasi, D. Henschel, P. J. Altmann, C. Jandl, S. Inoue, B. Rieger, *Angew. Chem. Int. Ed.* **2018**, *57*, 14575–14579; *Angew. Chem.* **2018**, *130*, 14783–14787; k) D. Wendel, D. Reiter, A. Porzelt, P. J. Altmann, S. Inoue, B. Rieger, *J. Am. Chem. Soc.* **2017**, *139*, 17193–17198; l) D. Reiter, P. Frisch, T. Szilvasi, S. Inoue, *J. Am. Chem. Soc.* **2019**, *141*, 16991–16996; m) D. Reiter, P. Frisch, D. Wendel, F. M. Hormann, S. Inoue, *Dalton Trans.* **2020**, *49*, 7060–7068; n) F. S. Tschernuth, F. Hanusch, T. Szilvási, S. Inoue, *Organometallics* **2020**, *39*, 4265–4272.

[11] J. Li, C. Schenk, C. Goedecke, G. Frenking, C. Jones, *J. Am. Chem. Soc.* **2011**, *133*, 18622–18625.

[12] a) P. Jutzi, C. Leue, *Organometallics* **1994**, *13*, 2898–2899; b) S. Inoue, M. Driess, *Organometallics* **2009**, *28*, 5032–5035; c) H. Lei, J. D. Guo, J. C. Fettinger, S. Nagase, P. P. Power, *Organometallics* **2011**, *30*, 6316–6322.

[13] Deposition Numbers 2086600 (for **1**), 2053426 (for **3**), 2053428 (for **4**), 2053429 (for **12**), and 2178695 (for **13**) contains the supplementary crystallographic data for this paper. These data are provided free of charge by the joint Cambridge Crystallographic Data Centre and Fachinformationszentrum Karlsruhe Access Structures service.

Manuscript received: June 21, 2022
Accepted manuscript online: August 4, 2022
Version of record online: August 25, 2022